Quantum dynamical tunneling breaks classical conserved quantities

Lingchii Kong (孔令琦),[1] Zongping Gong (龚宗平),[2] and Biao Wu (吴飙)[1,3,*]

[1]*International Center for Quantum Materials, School of Physics, Peking University, Beijing 100871, China*

[2]*Department of Applied Physics, University of Tokyo, 7-3-1 Hongo, Bunkyo-ku, Tokyo 113-8656, Japan*

[3]*Wilczek Quantum Center, School of Physics and Astronomy, Shanghai Jiao Tong University, Shanghai 200240, China*

(Received 29 January 2024; accepted 1 April 2024; published 13 May 2024)

We discover that quantum dynamical tunneling, occurring between phase space regions in a classically forbidden way, can break conserved quantities. We rigorously prove that a conserved quantity in a class of typical pseudointegrable systems can be broken quantum mechanically. We then numerically compute the uncertainties of this broken conserved quantity, which remain nonzero for up to 10^5 eigenstates and exhibit universal distributions similar to energy level statistics. Furthermore, all the eigenstates with large uncertainties show the superpositions of regular orbits with different values of the conserved quantity, showing definitive manifestation of dynamical tunneling. A random matrix model is constructed to successfully reproduce the level statistics of pseudointegrable systems.

DOI: 10.1103/PhysRevE.109.054113

I. INTRODUCTION

Dynamical tunneling is a fundamental quantum phenomenon which refers to classically forbidden transitions between phase-space regions, even without an energy barrier in the middle [1]. It has been well studied in both classically integrable and mixed systems (where integrable and chaotic phase-space regions coexist) within various contexts [2–13]. In such systems, dynamical tunneling was not observed to impact the overall integrability associated with the conserved quantities governing the entire system. In this paper, we use pseudointegrable systems to show that dynamical tunneling can break classical conserved quantities other than energy, giving rise to nonintegrable behaviors.

The pseudointegrable systems were introduced by Richens and Berry in 1981 [14]. They are defined as classical Hamiltonian systems with equal degrees of freedom and conserved quantities, where the phase trajectories are restricted to an invariant surface $\mathscr{R}$ featuring a multihandled sphere with genus larger than 1, in contrast to the genus-1 torus found in integrable systems. Typical examples of such systems are rational polygon billiards [see Fig. 1(a)], whose conserved quantity other than energy is given by

$$T(\cos\theta) \triangleq \cos(N\theta), \tag{1}$$

where θ is the angle between the momentum and the horizontal axis and N is the least common multiple of n_i for all vertices with rational angles $m_i\pi/n_i$ [15]. The conservation arises from the fact that the directions of each classical trajectory follow the orbits of a dihedral group D_N.

The dynamical properties of pseudointegrable systems have been studied over decades both classically and quantum mechanically but from very different perspectives. In classical mechanics, people are concerned about how the unremovable singularities on $\mathscr{R}$ split the beams of trajectories [14,15]. In the quantum counterpart, the exploration has primarily revolved around their energy level statistics [14,16–19]. Following this line, Bogomolny identified a subset of them characterized by the semi-Poisson distribution [20–25], which had been proposed as a universal intermediate bridging the gap between Poisson statistics and Wigner-Dyson statistics [26,27]. Pseudointegrable systems present two advantages for our study: (i) Singularities in phase space were suggested as an important element to provoke dynamical tunneling [3]; (ii) absence of a classical chaotic sea makes the nonintegrable behaviors more attributable to the effects of dynamical tunneling.

Here we focus on the rational right triangle billiards, as depicted in Fig. 1(b). This subclass has all the features of pseudointegrable systems. We analytically prove the absence of conserved quantity T in their quantum counterparts. The entire proof unfolds in two steps. First, assuming $\hat{T}$ as the quantization of T is conserved, we can expand the eigenstates by $2N$ plane waves with the directions following the orbits of group D_N. Second, imposing Dirichlet boundary conditions on the sides, we find that they cannot be satisfied, unless the billiards are completely integrable (see Appendix A for details).

To quantify the quantum mechanical breaking of the conserved quantity T, we calculate the uncertainty of operator $\hat{T}$ for each eigenstate, defined by

$$\sigma(\psi_n) \triangleq \langle\psi_n|\hat{T}^2|\psi_n\rangle - \langle\psi_n|\hat{T}|\psi_n\rangle^2, \tag{2}$$

where ψ_n denotes the nth eigenstate. We observe that the decreasing trend of $\sigma(\psi_n)$ with rising energy cannot be described by elementary functions. Instead, we examine the probability density functions (PDFs) of unfolded σ within an energy shell, revealing nontrivial distributions that can be accurately fitted by the Brody distribution [28,29]. The eigenstates with sufficiently small σ are collected and their unfolded level spacing statistics conform to the Poisson distribution, while the eigenstates with large σ showcase a

*wubiao@pku.edu.cn

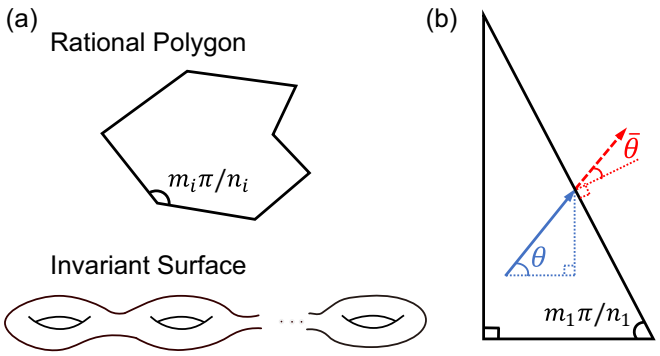

FIG. 1. Pseudointegrable systems. (a) Rational polygon and invariant surface $\mathscr{R}$ with constant energy and T. Each angle at the vertex i of polygon has a rational degree $m_i\pi/n_i$, with m_i and n_i being coprime integers. At least one vertex has $m_i > 1$. (b) Rational right triangle. m_1 and n_1 are coprime integers. The directions of momentum can be described by two alternative variables: the angle θ of inclination with respect to the horizontal axis or the included angle $\bar{\theta}$ with respect to the outer normal vector of sides.

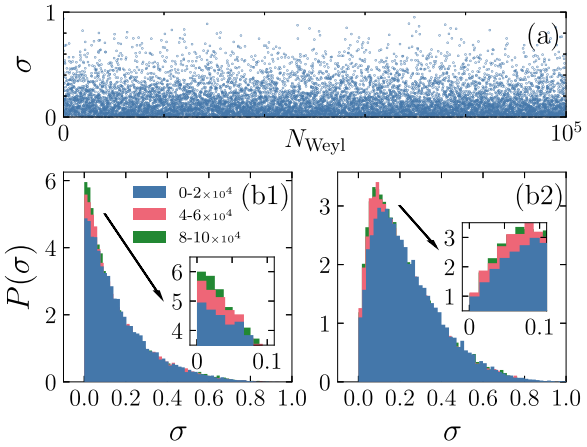

FIG. 2. (a) Scatter plots of σ in relation to N_{Weyl} for $\pi/8$ billiard, where 10^4 points are sampled uniformly. (b1), (b2) PDFs of σ. The 10^5 eigenstates are categorized into three groups based on their energy levels, with three different colors representing N_{Weyl} within the ranges of 0–2 × 10^4, 4–6 × 10^4, and 8–10 × 10^4. The insets provide a closer look at σ smaller than 0.1. Notably, (b1) and (b2) respectively correspond to $\pi/8$ and $\pi/7$ billiards.

superposition with classical regular orbits with different T, regardless of whether they are periodic or not. It is the consequence of dynamical tunneling, which results in avoided crossings among regular states. Inspired by the statistics of σ, we develop a random matrix model for dynamical tunneling and successfully reproduce the level spacing distributions of pseudointegrable systems.

II. CONSERVED QUANTITY

Each classical trajectory has directions being the orbits of dihedral group D_N, which fold $0 \leqslant \theta \leqslant 2\pi$ into an interval $[0, \pi/N]$. This corresponds to a quotient map $|\theta \bmod (2\pi/N)|$, functioning as a conserved quantity [15]. For simplicity, we use the form (1). This choice stems from the fact that $\cos(N\theta)$ can be expanded in terms of $\cos\theta$ using the Nth-order Chebyshev polynomials of the first kind and $\cos\theta$ can be easily quantized as $\hat{P}_x/\hat{P}$, where $\hat{P}$ is the magnitude of the momentum and $\hat{P}_x$ is the momentum operator along the x direction. Consequently, the classical trajectory in phase space can be projected onto $\mathscr{R}$. It is simple to prove $T(\cos\theta)$ is conserved along a classical trajectory, i.e., for a certain reflection at one side, $T(\cos\theta) = \cos(N\theta) \to \cos[N(2j\pi/N \pm \theta)] = \cos(N\theta) = T(\cos\theta)$ for $j = 0, 1, \ldots, N-1$. The quantization result can be exemplified by considering the case of an integrable isosceles right triangle billiard, where $N = 4$. In this case, the operator $\hat{T}$ is represented by the expression $\hat{T} = 8(\hat{P}_x/\hat{P})^4 - 8(\hat{P}_x/\hat{P})^2 + 1$. When the operator $\hat{P}_x/\hat{P}$ acts on $|\psi_n\rangle$, it yields $\hat{P}_x|\psi_n\rangle/(\hbar k_n)$, where k_n is the wave number of ψ_n.

III. UNCERTAINTY

We calculate the quantum right triangle billiards with one interior angle being $\pi/8$, $\pi/5$, $\pi/7$, $2\pi/7$, $\pi/9$, $2\pi/9$ (these angles are used to represent the corresponding billiards in the following parts). The genus of $\mathscr{R}$ is given by the formula $1 + N\sum_i (m_i - 1)/(2n_i)$. Consequently, each pair of billiards corresponds to $\mathscr{R}$ with genus-2, 3, 4. It is noted that the energy level statistics of $\pi/8$ and $\pi/5$ has been found to be semi-Poisson distribution [20]. For each billiard, 10^5 eigenstates are calculated using a hybrid of scaling method and decomposition method [30,31]. We use Weyl's level N_{Weyl} to indicate the energy of eigenstates, $N_{\text{Weyl}} = (Sk_n^2 - Lk_n)/(4\pi)$, where S and L are the area and perimeter of billiard tables, respectively [32]. It helps to compare different systems with a unified energy scale.

The direct results of σ are depicted in Fig. 2(a). It demonstrates that most points cluster around the small values of σ. However, there are still eigenstates with large σ values at higher energy levels. Since σ does not exhibit a clear decreasing trend with N_{Weyl}, we analyze σ statistically. If $\hat{T}$ were conserved, we would expect the PDF of uncertainties, denoted as $P(\sigma)$, to be a delta distribution at $\sigma = 0$. However, the statistical results show that $P(\sigma)$ follow various nontrivial distributions. This is exemplified by $\pi/8$ and $\pi/7$ billiards in Figs. 2(b1) and 2(b2). Both $P(\sigma)$ have right tails but different peaks. With energy rising, they exhibit a trend to converge to delta distribution. It indicates that, in the classical limit, the conserved quantity T will recover.

To gain further insights, we consider the unfolded uncertainty, defined as $\widetilde{\sigma} \triangleq \sigma/\text{mean}(\sigma)$, where $\text{mean}(\sigma)$ represent the mean value of the ensemble $\{\sigma(\psi_n)\}$. The domain is extended from $\sigma \in [0, 1]$ to $\widetilde{\sigma} \in [0, \infty]$, because $\text{mean}(\sigma)$ can be arbitrarily small. The PDFs of $\widetilde{\sigma}$, denoted as $P(\widetilde{\sigma})$, are shown in Fig. 3(a). All $P(\widetilde{\sigma})$ presented here can be well fitted by Brody distributions $P_{\text{Brody}}(\widetilde{\sigma}) = a(q+1)\widetilde{\sigma}^q \exp(-a\widetilde{\sigma}^{q+1})$, $a = \Gamma[(q+2)/(q+1)]^{q+1}$ with a single parameter $q \in [0, 1]$. In particular, for $\pi/8$ and $\pi/5$ billiards, whose level statistics are semi-Poissonian, $P(\widetilde{\sigma})$ closely resemble the $q = 0$ Poisson distribution $\exp(-\widetilde{\sigma})$. The differences in cumulative distribution functions (CDFs) from the best-fitted model, denoted by $U_B(\widetilde{\sigma}) := \int_0^{\widetilde{\sigma}} d\widetilde{\sigma}_1[P(\widetilde{\sigma}_1) - P^*_{\text{Brody}}(\widetilde{\sigma}_1)]$ where the superscript

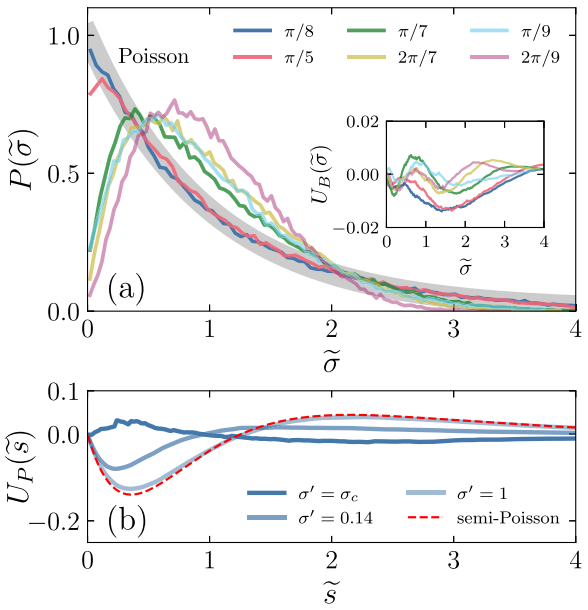

FIG. 3. (a) PDFs of $\widetilde{\sigma}$ for 10^5 eigenstates. The shaded band represents Poisson distribution, i.e., $\exp(-\widetilde{\sigma})$. These distributions are fitted by the Brody distribution. The inset displays the differences in CDFs from their optimal fitting distributions, denoted as $U_B(\widetilde{\sigma})$. The optimal fitting parameters q are approximately 1.0, 1.0, 1.4, 1.5, 1.5, 1.9 for $\pi/8$, $\pi/5$, $\pi/7$, $2\pi/7$, $\pi/9$, $2\pi/9$ billiards, respectively. (b) Differences in CDFs of unfolded level spacing with different uncertainty thresholds from the Poisson distribution, denoted as $U_P(\widetilde{s})$. σ' is the selected threshold value. For $\pi/8$ billiard, σ_c is chosen to be 0.0189 with the number of pseudoregular states amounting to 11481. Notably, in the absence of uncertainty threshold ($\sigma' = 1$), the level spacing distribution for the whole spectrum follows $P_{\text{semi-Poisson}}(\widetilde{s})$, as indicated by the red dashed line. Additionally, the level spacing distribution for the uncertainties less than 0.14 is shown at the intermediate position between Poisson and semi-Poisson distribution.

$*$ represents "optimal fitting," are shown in the inset, which give the errors less than 2%. This result shows that $P(\widetilde{\sigma})$ for genus-3, 4 billiards have a polynomial repulsion at small $\widetilde{\sigma}$ and a superexponential tail at large $\widetilde{\sigma}$. Roughly, $P(\widetilde{\sigma})$ exhibits an elevated q with genus increasing, as shown in Fig. 3(a). This may be understood from Diophantine approximations. Consider a right triangle billiard, as depicted in Fig. 1(b), where the ratio m_1/n_1 is a good Diophantine approximation of some irrational number. Then, N is typically large, resulting in a high genus. Since irrational triangle billiards lack the conserved quantity T, an $\mathscr{R}$ with higher genus naturally implies a more chaotic system.

To confirm our expectation that the level statistics of eigenstates with small enough σ follows a Poisson distribution, we scan the values of σ to determine a small enough threshold σ_c, such that the unfolded level spacing distribution of eigenstates with $\sigma < \sigma_c$ aligns with the Poisson distribution with minimal fitting error. This can be formulated as $P(\widetilde{s}\,|\{\psi_n, \sigma(\psi_n) < \sigma_c\}) \simeq P_{\text{Poisson}}(\widetilde{s})$, where $P_{\text{Poisson}}(\widetilde{s}) = \exp(-\widetilde{s})$ and $\widetilde{s}$ is the unfolded level spacing. We call the eigenstates with $\sigma < \sigma_c$ "pseudoregular" states. The results for $\pi/8$ billiard are depicted in Fig. 3(b), where the differences in CDFs of unfolded level spacing with different thresholds σ' from the Poisson distribution are calculated, defined as $U_P(\widetilde{s}) := \int_0^{\widetilde{s}} d\widetilde{s}_1[P(\widetilde{s}_1\,|\{\psi_n, \sigma(\psi_n) < \sigma'\}) - P_{\text{Poisson}}(\widetilde{s}_1)]$. It shows that the level statistics of pseudoregular states approximates to $P_{\text{Poisson}}(\widetilde{s})$, implying an absence of level repulsions in the spectrum if $\hat{T}$ is conserved. It is established that, when all the eigenstates are involved ($\sigma' = 1$), the level spacing statistics for the whole spectrum follows a semi-Poisson distribution, i.e., $P_{\text{semi-Poisson}}(\widetilde{s}) = 4\widetilde{s}\exp(-2\widetilde{s})$. By increasing the threshold to $\sigma' = 0.14 > \sigma_c$, the level statistics occupies an intermediate position between the Poisson and semi-Poisson distribution. This demonstrates that, by controlling the uncertainty threshold σ', the level statistics can be changed between these two distributions. We will see that the eigenstates with $\sigma > \sigma_c$ are characterized by the superposition of classical trajectories with distinct values of T, which is induced by dynamical tunneling.

IV. DYNAMICAL TUNNELING

The direct approach to investigate dynamical tunneling is mapping the eigenstates into phase space [33–35]. Fortunately, in pseudointegrable systems, each classical orbit has a specific value of T. As a result, each eigenstate that may be a superposition of different classical orbits can be converted into a distribution of different T values. This distribution is expressed by the boundary function $u_n(\bar{\theta})$ of ψ_n, where $\bar{\theta}$ is the included angle between the outer normal vector of sides and the momentum as shown in Fig. 1(b). $u_n(\bar{\theta})$ can be obtained by two steps. First, we choose the Poincaré section as the boundary of a billiard table. Then, the wave function on boundary u_n' can be evaluated as the normal derivative of ψ_n, i.e., $u_n'(s) \triangleq \hat{\mathbf{n}}(s)\cdot\nabla\psi_n(x(s), y(s))$, where $(x(s), y(s))$ is a point on the boundary parametrized by the arc length s and $\hat{\mathbf{n}}(s)$ is the outer normal unit vector at $(x(s), y(s))$. Secondly, we perform the Fourier transformation of $u_n'(s)$ to obtain its conjugate function $u_n(\bar{\theta})$, i.e., $u_n(\bar{\theta}) = \oint_{\partial B} ds\, \exp(ik_n s\,\sin\bar{\theta})u_n'(s)$, where ∂B is the boundary curve. The details are given in Appendix B or Ref. [36]. With $\bar{\theta}$, the conserved quantity T can be rewritten as $T = |T(\cos\bar{\theta})| = |\cos(N\bar{\theta})|$, where the absolute value arises at the hypotenuse $\bar{\theta} = \pi/2 + m\pi/n - \theta$. In this way, $\bar{\theta}$ becomes the connection between $u_n(\bar{\theta})$ and T.

The results of the $\pi/8$ billiard are shown in Fig. 4. For this billiard, there are only two types of classical orbits: periodic orbits (POs) and uniformly distributed orbits (UDOs) that cover the entire billiard table [37]. It has been established that, in rational right triangle billiards, nearly every periodic orbit contains segments that are perpendicular to a specific side. Consequently, almost all POs have $T = 1$, while UDOs have various values of T. Quantum mechanically, there exists "superscar" states, named by Bogomolny [22,38,39], exhibiting a superposition of spatially parallel POs. T cannot be used to distinguish different superscar states as they are all equal to 1.

In both Figs. 4(a) and 4(b), $|u_n(\bar{\theta})|^2$ exhibit a single peak, illustrating the features of superscar and UDO, respectively. Both of them are pseudoregular states, characterized by uncertainties σ smaller than σ_c. However, in Figs. 4(c1) and 4(d1), orbits with different values of T are superposed [one superscar plus one UDO in (c1) and two UDOs in (d1)], causing their relatively large σ. Notably, eigenstates with small wave numbers may distribute with a considerable width on

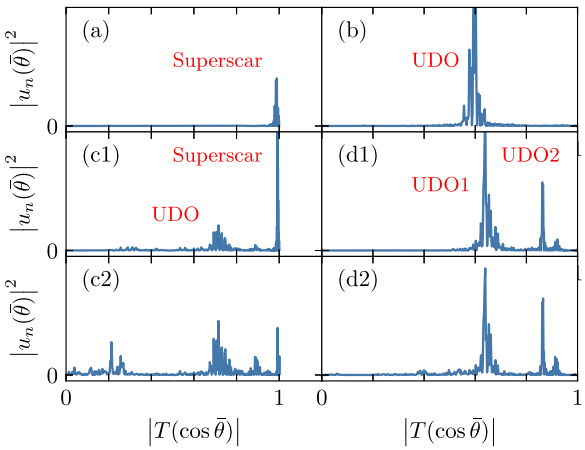

FIG. 4. Profiles of different types of eigenstates for $\pi/8$ billiard, illustrated by $u_n(\bar{\theta})$ with respect to $|T(\cos\bar{\theta})|$. (a) Superscar state with $N_{\text{Weyl}} \approx 10017.3$ and $\sigma \approx 0.006$. (b) Spatial uniformly distributed orbit with $N_{\text{Weyl}} \approx 40090.0$ and $\sigma \approx 0.002$. (c1) Superposition of a single superscar and a single UDO with $N_{\text{Weyl}} \approx 60144.6$ and $\sigma \approx 0.563$. Panel (c2) is the eigenstate next to (c1) with $N_{\text{Weyl}} \approx 60144.1$ and $\sigma \approx 0.489$. (d1) Superposition of two UDOs with $N_{\text{Weyl}} \approx 61476.4$ and $\sigma \approx 0.461$. Panel (d2) is the eigenstate next to (d1) with $N_{\text{Weyl}} \approx 61476.6$ and $\sigma \approx 0.509$.

the values of T, leading to an elevated σ. But the presence of separated peaks here eliminates this concern. The eigenstates neighboring to Figs. 4(c1) and 4(d1) are shown in Figs. 4(c2) and 4(d2). And each pair of them shares common peak positions, signifying common tunneled components. Additionally, their individual level splittings are much smaller than the mean level spacing 1. This is another indication of dynamical tunneling. In Fig. 4(c2), there emerge subpeaks at small T comparing to Fig. 4(c1), which may illustrate more resonant orbits. Therefore, the results indicate that dynamical tunneling destroys the conservation of $\hat{T}$ by superposing trajectories with different directions.

V. AVOIDED CROSSING

The dynamical tunneling can be modeled by a random matrix Hamiltonian

$$h = \begin{pmatrix} \varepsilon & \gamma \\ \gamma & -\varepsilon \end{pmatrix}, \tag{3}$$

where the diagonals $\pm\varepsilon$ are energy levels of classical orbits with different values of T and the off-diagonal γ represent tunneling rates between these. γ is real due to the time-reversal symmetry. As different classical orbits are not correlated [as shown in Fig. 3(b)], it is reasonable to assume that ε has a Poisson distribution, i.e., $P(\varepsilon) = \exp(-2|\varepsilon|)$.

We reproduce the level spacing distribution of $\pi/8$ or $\pi/5$ billiard, which is already known to be $P_{\text{semi-Poisson}}(\widetilde{s})$. Suggested by Figs. 2(b1) and 3(a), we semiempirically estimate that the distribution $g(\gamma)$ of γ has an exponential shape similar to $P(\widetilde{\sigma})$, specifically,

$$g(\gamma) = g(-\gamma) \approx \tfrac{1}{2}\exp(-|\gamma|). \tag{4}$$

Once $P(\varepsilon)$ and $g(\gamma)$ are known, we can compute the unfolded level spacing distribution of (3), which is compared with

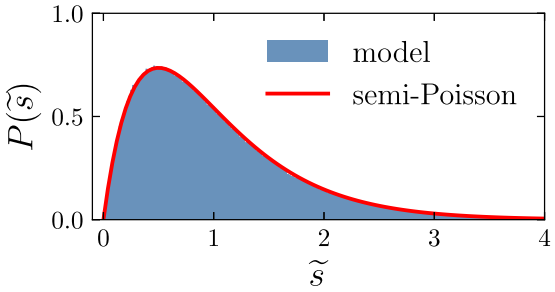

FIG. 5. Unfolded level spacing distribution of model (3) using the tunneling rate (4). The level spacings are collected from 10^6 ensembles. The red line represents the semi-Poisson distribution.

$P_{\text{semi-Poisson}}(\widetilde{s})$ in Fig. 5, demonstrating a perfect fit. Therefore, combining the results in Figs. 3(b) and 5, we can conclude that dynamical tunneling is responsible for distorting the level spacing distribution from a Poisson distribution to the semi-Poisson distribution. We expect this mechanism applies to all pseudointegrable systems with diverse level spacing distributions.

VI. DISCUSSION

The dynamical tunneling observed in pseudointegrable systems shows different effects compared to those in integrable and mixed systems. We break them down into three aspects. (i) Conserved quantity. In mixed systems, one can define a "local" conserved quantity for the trajectories within symmetry-related integrable islands. Dynamical tunneling among these integrable islands or from them into the chaotic sea can destroy this local conserved quantity [3–13]. However, here, dynamical tunneling has the potential to break the conserved quantity T governing the entire systems by superposing classical orbits with different values of T (as shown in Figs. 2 and 4). (ii) Level statistics. For mixed systems, dynamical tunneling can only introduce subleading corrections to the Berry-Robnik level statistics, since it weakly couples regular and chaotic states, thus increasing small distances between the corresponding levels [4–8,40]. The level repulsion in pseudointegrable systems is completely induced by dynamical tunneling [as shown in Fig. 3(b)]. (iii) Tunneling rate. In principle, the tunneling rate between two resonant "double-well states" decreases exponentially with $\hbar^{-1}$, which can be expressed as $\ln\gamma \propto -\xi\hbar^{-1} + O(\ln\hbar)$, where ξ is a parameter related to systems and resonant orbits (for a double-well system, ξ is the imaginary part of action over the energy barrier in the middle) [3,4,41]. In the presence of more resonant states, the tunneling rates between the original pair can be enhanced or suppressed by several orders of magnitude at certain values of $\hbar^{-1}$ [9–13]. We formulate this qualitatively as $\xi = \xi(\hbar^{-1}) = \bar{\xi} + \sum_i \lambda_i \delta(\hbar^{-1} - \hbar_i^{-1})$, where $\bar{\xi}$ is the average value over a shell of $\hbar^{-1}$, $\hbar_i^{-1}$ is the enhanced (or suppressed) point, and λ_i is the corresponding strength. In the limit of strong tunneling, the distribution of $\hbar_i^{-1}$ becomes dense on the shell, allowing us to treat ξ as a random variable centered around $\bar{\xi}$. This is consistent with our semiempirical distribution of tunneling rate (4). However, a rigorous quantitative derivation of the tunneling rate remains an open problem.

ACKNOWLEDGMENTS

We thank M. Berry, L. Ying, and L. Huang for helpful discussions. L.K. and B.W. are supported by the National Natural Science Foundation of China (Grants No. 111921005 and No. 192365202) and Shanghai Municipal Science and Technology Major Project (Grant No. 2019SHZDZX01). Z.G. is supported by The University of Tokyo Excellent Young Researcher Program.

APPENDIX A: PROOF OF CONSERVED QUANTITY BREAKING IN RATIONAL RIGHT TRIANGLE BILLIARDS

Consider a rational right triangle billiard described in Fig. 6. The direction θ can undergo three kinds of reflections by sides: $\theta \to -\theta$ (reflection at $y = 0$), $\theta \to \pi - \theta$ (reflection at $x = L\cos\alpha$), and $\theta \to 2\alpha - \theta$ (reflection at $y = x\tan\alpha$). These can generate a dihedral group D_N ($N = n_1$) with dimension $2N$, yielding a conserved quantity $T = \cos N\theta$ independent with the energy. T can be quantized after expanding to the polynomial of $\cos\theta = P_x/P$, where P_x is the momentum along the x direction and P is the magnitude of total momentum.

The conserved quantity T originates from the existence of quotient projection mapping each classical trajectory on the surface S^1/D_N, where S^1 is the unit circle. It means that, for a classical trajectory, the possible directions, denoted as $\pm\theta_j$, can be related to a reference $\theta_0 \in [0, \pi/N]$ so that

$$\theta_j = \theta_0 + \frac{2j\pi}{N}, \quad j = 0, 1, \ldots, N-1. \tag{A1}$$

If the quantized operator $\hat{T}$ remains conserved in quantum mechanics, the eigenstate should also follow the orbits of group D_N, just as each classical trajectory does. In this manner, the eigenstate, denoted as $|\psi\rangle$, can be expanded by plane waves with direction $\pm\theta_j$,

$$|\psi\rangle = \sum_{j=0}^{N-1}(c_j^+|k\cos\theta_j, k\sin\theta_j\rangle + c_j^-|k\cos\theta_j, -k\sin\theta_j\rangle), \tag{A2}$$

where $c_j^\pm$ are the superposing parameters. Then, the Dirichlet boundary conditions at $y = 0$, $y = x\tan\alpha$, and $x = L\cos\alpha$ can be evaluated sequentially:

$$\sum_{j=0}^{N-1}(c_j^+ + c_j^-)e^{ikx\cos\theta_j} = 0, \tag{A3}$$

$$\sum_{j=0}^{N-1}[c_j^+ e^{ikr\cos(\theta_j-\alpha)} + c_j^- e^{ikr\cos(\theta_j+)}] = 0, \tag{A4}$$

$$\sum_{j=0}^{N-1}(c_j^+ e^{iky\sin\theta_j} + c_j^- e^{-iky\sin\theta_j})e^{ikL\cos\alpha\cos\theta_j} = 0, \tag{A5}$$

where $r = \sqrt{x^2+y^2} \in [0, L]$. Suppose the subscript of $c_j^\pm$ has a cyclic relation $c_j^\pm := c_{j \bmod N}^\pm$ for $j \in \mathbb{Z}$; Eq. (A4) can be rewritten as

$$\sum_{j=0}^{N-1}(c_{j+m}^+ + c_j^-)e^{ikr\cos(\theta_j+\alpha)} = 0. \tag{A6}$$

We can prove that Eq. (A3) and Eq. (A6) are equivalent to

$$c_j^+ + c_j^- = c_{j+m}^+ + c_j^- = 0, \quad j = 0, 1, \ldots, N-1. \tag{A7}$$

We take the ith ($i = 1, 2, \ldots, N-1$) derivative of the both sides of Eq. (A3) and make x equal to zero. In this way, we obtain N homogeneous linear equations by defining $a_j := c_j^+ + c_j^-$,

$$\begin{bmatrix} 1 & 1 & \cdots & 1 \\ \cos\theta_0 & \cos\theta_1 & \cdots & \cos\theta_{N-1} \\ \cos^2\theta_0 & \cos^2\theta_1 & \cdots & \cos^2\theta_{N-1} \\ \vdots & \vdots & \ddots & \vdots \\ \cos^{N-1}\theta_0 & \cos^{N-1}\theta_1 & \cdots & \cos^{N-1}\theta_{N-1} \end{bmatrix} \begin{bmatrix} a_0 \\ a_1 \\ \vdots \\ a_{N-1} \end{bmatrix} = 0. \tag{A8}$$

Its determinant is known as the Vandermonde determinant, yielding

$$\det[\cos^{i-1}\theta_j]_{N\times N} = \prod_{0\leqslant i<j\leqslant N-1}(\cos\theta_j - \cos\theta_i). \tag{A9}$$

If we let $\cos\theta_j = \cos\theta_i$, we obtain $\theta_0 = (N-i-j)\pi/N$, which cannot be confined in the domain $(0, \pi/N)$. As a result, this determinant is nonzero for $\theta_0 \in (0, \pi/N)$. In this way, the solution to Eq. (A8) is a null vector, i.e.,

$$a_j = c_j^+ + c_j^- = 0. \tag{A10}$$

When $\theta_0 = 0, \pi/N$, the billiard has N directions corresponding to degenerate cases with $\theta_j = -\theta_{N-j}$. We redefine the superposing parameter as c_j, so that

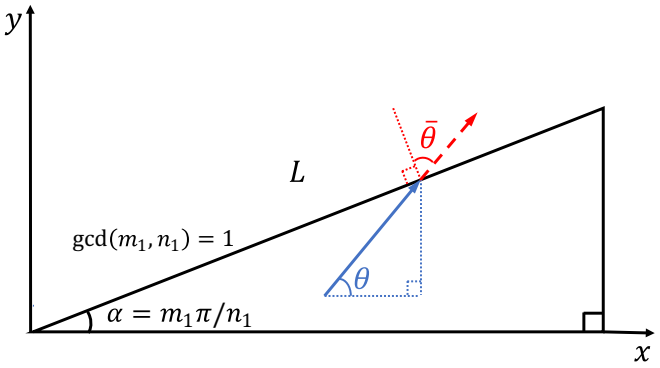

FIG. 6. Rational right triangle billiard. This billiard includes at least one vertex with angle α being $m_1\pi/n_1$, where n_1 is even and m_1 ($m_1 \neq 1$) and n_1 are coprime integers. L is the length of the hypotenuse. The directions of billiard can be described by either of two alternative variables: the angle θ of inclination with respect to the x axis or the included angle $\bar{\theta}$ with respect to the outer normal vector of sides.

$|\psi\rangle = \sum_{j=0}^{N-1} c_j |k\,\cos\theta_j, k\,\sin\theta_j\rangle$. For $\theta_0 = 0$, the degenerate versions of boundary conditions Eq. (A3) and Eq. (A4) become

$$c_0 e^{ikx} + c_{N/2} e^{-ikx} + \sum_{j=1}^{N/2-1} (c_j + c_{N-j}) e^{ikx\,\cos\theta_j} = 0, \tag{A11}$$

$$\sum_{j=0}^{(m-1)/2} (c_j + c_{m-j}) e^{ikr\cos(\theta_j-\alpha)} + \sum_{j=m+1}^{(m+N-1)/2} (c_j + c_{m+N-j}) e^{ikr\cos(\theta_j-\alpha)} = 0. \tag{A12}$$

These two relations are equivalent to $c_j + c_{N-j} = c_j + c_{m-j} = 0$, yielding $c_{m-j} = c_{-j}$. Consequently, all c_j must equal $c_0 = 0$. For $\theta_0 = \pi/N$, we have

$$\sum_{j=0}^{N/2-1} (c_j + c_{N-1-j}) e^{ikx\,\cos\theta_j} = 0, \tag{A13}$$

$$c_{(m-1)/2} e^{ikr} + c_{(m+N-1)/2} e^{-ikr} + \sum_{j=0}^{(m-3)/2} (c_j + c_{m-1-j}) e^{ikr\cos(\theta_j-\alpha)} + \sum_{j=m}^{(m+N-3)/2} (c_j + c_{m+N-1-j}) e^{ikr\,\cos(\theta_j-\alpha)} = 0. \tag{A14}$$

They are equivalent to $c_j + c_{N-j-1} = c_j + c_{m-j-1} = 0$, yielding $c_{m-j-1} = c_{1-j}$. Consequently, all c_j must equal $c_{(m-1)/2} = 0$. So far, we have proved an absence of common eigenstates for the degenerate cases of $\theta_0 = 0, \pi/N$.

Using the same tricks on Eq. (A6), we can obtain $c^+_{j+m} + c^-_j = 0$.

Applying the relation Eq. (A7) on the eigenstates $|\psi\rangle$, we get

$$\psi(x,y) = \sum_{j=0}^{N/2-1} \sin(kx\,\cos\theta_j)\sin(ky\,\sin\theta_j). \tag{A15}$$

One can verify $\psi(x,y)$ is invariant under the action of dihedral group D_N, $\theta_j \to 2\beta\pi/N \pm \theta_j$ for $\beta \in \mathbb{Z}$. $\psi(x,y)$ is an irreducible representation of group D_N.

We apply the boundary condition Eq. (A5) to Eq. (A15), yielding

$$\sum_{j=0}^{N/2-1} \sin(kL\,\cos\alpha\,\cos\theta_j)\sin(ky\,\sin\theta_j) = 0. \tag{A16}$$

We can prove that Eq. (A16) is equivalent to

$$\sin(kL\cos\alpha\cos\theta_j) = 0 \quad \text{or} \quad kL\cos\alpha\cos\theta_j = M_j\pi, \tag{A17}$$

where $M_j \in \mathbb{Z}, \forall j = 0, 1, \ldots, N/2-1$. This proof is similar to the proof of Eq. (A7). We take the $(2i-1)$th ($i = 1, 2, \ldots, N/2$) derivatives of both sides of Eq. (A11) and make y equal to zero. We obtain $N-1$ homogeneous linear equations by defining $b_j := \sin(kL\,\cos\alpha\,\cos\theta_j)\sin\theta_j$,

$$\begin{bmatrix} 1 & 1 & \ldots & 1 \\ \sin^2\theta_0 & \sin^2\theta_1 & \ldots & \sin^2\theta_{N-1} \\ \sin^4\theta_0 & \sin^4\theta_1 & \ldots & \sin^4\theta_{N-1} \\ \vdots & \vdots & \ddots & \vdots \\ \sin^{N-2}\theta_0 & \sin^{N-2}\theta_1 & \ldots & \sin^{N-2}\theta_{N-1} \end{bmatrix} \begin{bmatrix} b_0 \\ b_1 \\ \vdots \\ b_{N-1} \end{bmatrix} = 0. \tag{A18}$$

Its determinant is nonzero, so the solution is $b_j = 0$, yielding $\sin(KL\,\cos\alpha\,\cos\theta_j) = 0$.

The relation Eq. (A17) can be used as the quantization condition. We divide it by itself with a different subscript and obtain

$$\frac{\cos\theta_j}{\cos\theta_{j'}} = \frac{M_j}{M_{j'}} \in \mathbb{Q}, \quad j, j' = 0, 1, \ldots, N-1, \tag{A19}$$

where $M_j = -M_{N-j-1}$ for $j = N/2, N/2+1, \ldots, N-1$. By using the identity

$$\cos\theta_j + \cos\theta_{j'} = 2\,\cos\frac{\theta_j + \theta_{j'}}{2}\cos\frac{\theta_j - \theta_{j'}}{2} \tag{A20}$$

and setting j' to be $j+2$, we find that

$$2\,\cos\frac{2\pi}{N} = \frac{\cos\theta_j}{\cos\theta_{j+1}} + \frac{\cos\theta_{j+2}}{\cos\theta_{j+1}} \in \mathbb{Q}, \tag{A21}$$

illustrating the left-hand side (LHS) is rational. It is known that if the cosine of a rational angle is a rational number, the only possible cosine values are $\pm 1, \pm 1/2$, and 0 (a proof was provided in [42]). They correspond to the right triangle billiards with $\alpha = \pi/6$ and $\pi/4$, which are the only two complete integrable cases. For others, Eq. (A21) is not satisfied. Therefore, we conclude that, in rational right triangle billiards, $\hat{T}$ is not conserved unless the billiards are integrable.

APPENDIX B: POINCARÉ-HUSIMI REPRESENTATION

Poincaré-Husimi representation is used to compare the eigenstates with classical trajectories [36,43]. In this representation, the Poincaré section is typically chosen at the boundary of billiards, yielding the boundary function defined as the normal derivative of eigenfunction, i.e.,

$$u'_n(s) \triangleq \hat{\mathbf{n}}(s) \cdot \nabla\psi_n(x(s), y(s)), \tag{B1}$$

where $(x(s), y(s))$ is a point on the boundary parametrized by the arc length s and $\hat{\mathbf{n}}(s)$ denotes the outer normal unit vector at $(x(s), y(s))$. Conversely, the wave function can be obtained

by boundary integral

$$\psi_n(x,y) = -\oint_{\partial B} ds\, u_n'(s) G[x,y;x(s),y(s)], \tag{B2}$$

where ∂B is the billiard boundary curve, (x,y) is the point inside the billiard table, and $G[x,y;x(s),y(s)]$ is the two-dimensional free particle Green's function. In phase space, the conjugate variable to s is $\sin\bar{\theta}$, where $\bar{\theta}$ represents the included angle between the outer normal vector of sides and the velocity of billiard flow, as shown in Fig. 6. The conjugate function $u_n(\bar{\theta})$ is expressed as

$$u_n(\bar{\theta}) = \oint_{\partial B} ds\, \exp(iks\,\sin\bar{\theta}) u_n'(s), \tag{B3}$$

where k is the wave number. It should be emphasized that the relations between θ and $\bar{\theta}$ have three kinds depending on the sides: $\bar{\theta} = \theta + \pi/2$ (for $y = 0$), $\bar{\theta} = \theta$ (for $x = L\cos\alpha$), and $\bar{\theta} = \pi/2 + \alpha - \theta$ (for $y = x\tan\alpha$). Hence $|T(\cos\bar{\theta})|$ remains the classical conserved quantity. Without ambiguity, we also use the symbol T to denote $|T(\cos\bar{\theta})|$. The values of T can be used to distinguish different trajectories. For example, in the $\pi/8$ billiard, there are only two types of classical orbits: periodic orbits (POs) and uniformly distributed orbits (UDOs) that cover the entire billiard table. It has been established that almost each PO possesses segments perpendicular to the side of the right triangle. Consequently, almost all POs have $T = 1$, while UDOs have various values of T. Quantum mechanically, there exists "superscar" states, exhibiting a superposition of spatially parallel POs. T cannot be used to distinguish different superscar states as they all equal 1. But the complete details of trajectories can be obtained by projecting the eigenstate using Husimi functions on the phase space expanded by s and $\sin\bar{\theta}$.

The Husimi function $h(q,p)$ with $q = s$, $p = \sin\bar{\theta}$ is defined as

$$h(q,p) \triangleq \frac{1}{A}\left|\oint_{\partial B} c^k_{(q,p)}(l) u_n'(l) dl\right|^2, \tag{B4}$$

where A is the normalization parameter. $c^k_{(q,p)}(l)$ is the standard coherent state, i.e.,

$$c^k_{(q,p)}(l) = \sum_{j\in\mathbb{Z}} \exp[ikp(l-q+j\mathscr{L})] \times \exp\left[-\frac{k}{2}(l-q+j\mathscr{L})^2\right], \tag{B5}$$

where $\mathscr{L}$ is the length of the boundary and the sum of j ensures the coherent states being periodic with a period of $\mathscr{L}$.

The results for the $\pi/8$ billiard are shown in Fig. 7. And the Poincaré-Husimi representations and the plot of the conjugate boundary function $u_n(\bar{\theta})$ with respect to the conserved quantity T are compared to illustrate the trajectories of typical eigenstates with different σ (the uncertainty of $\hat{T}$). The eigenstate in Fig. 7(a) is a superscar state, superposed by two parallel POs with segments perpendicular to the hypotenuse. The eigenstate in Fig. 7(b) illustrates a UDO. Both of these are pseudoregular states, each exhibiting a single peak at the corresponding value of T and thus possessing the conserved quantity $\hat{T}$. The eigenstate in Fig. 7(c1) is a superposition of one superscar (including four parallel POs) and one UDO

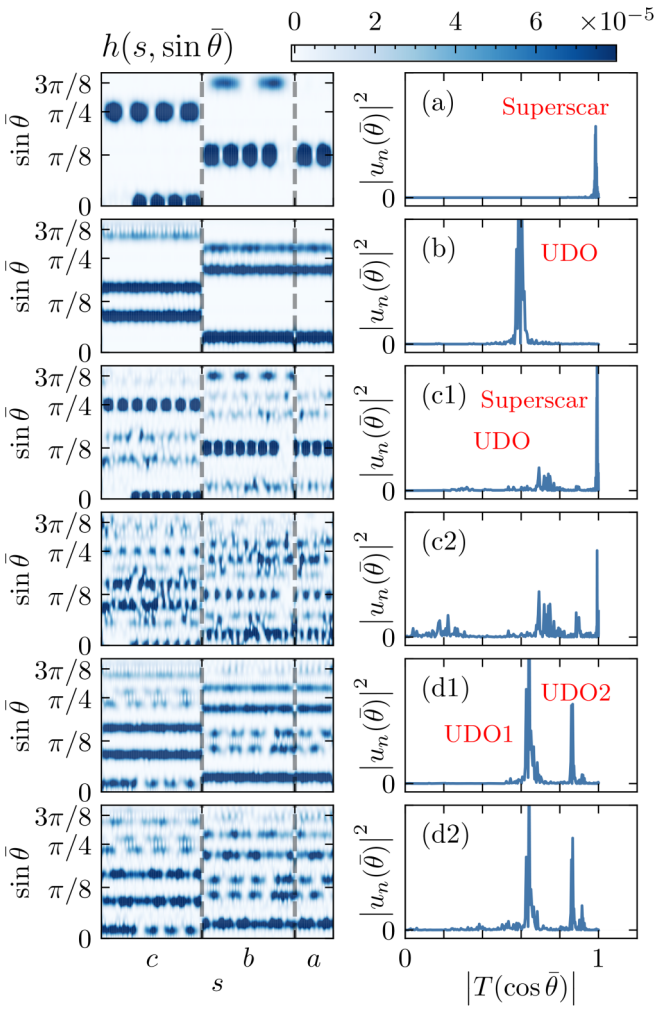

FIG. 7. Trajectories of typical eigenstates for the $\pi/8$ billiard. The left column are the distributions of Husimi functions $h(s,\sin\bar{\theta})$ on the phase space spanned by s and $\sin\bar{\theta}$. c, b, and a respectively represent the hypotenuse, the adjacent side, and the opposite side of the $\pi/8$ corner. The right column is the conjugate boundary function $u_n(\bar{\theta})$ with respect to the conserved quantity $|T(\cos\bar{\theta})|$. Each row corresponds to the same eigenstate. (a) A superscar state with $N_{\text{Weyl}} \approx 10017.3$ and $\sigma \approx 0.006$, typically exhibiting a superposition of parallel periodic orbits. (b) A spatial uniformly distributed orbit with $N_{\text{Weyl}} \approx 40090.0$ and $\sigma \approx 0.002$. (c1) A superposition of a single superscar and a single UDO with $N_{\text{Weyl}} \approx 60144.6$ and $\sigma \approx 0.563$. Panel (c2) is the eigenstate next to (c1) with $N_{\text{Weyl}} \approx 60144.1$ and $\sigma \approx 0.489$. (d1) A superposition of two UDOs with $N_{\text{Weyl}} \approx 61476.4$ and $\sigma \approx 0.461$. Panel (d2) is the eigenstate next to (d1) with $N_{\text{Weyl}} \approx 61476.6$ and $\sigma \approx 0.509$.

from the observation on $h(s,\sin\bar{\theta})$. Consequently, it has two separated peaks on the distribution of T, causing an elevated σ. The eigenstate in Fig. 7(c2), which is next to the one in Fig. 7(c1), includes the trajectories in Fig. 7(c1) plus an additional UDO [this UDO also exists in Fig. 7(c1) but with a minimal peak]. The eigenstates in Figs. 7(d1) and 7(d2) are another pair with the energy splitting much smaller than the mean level spacing and exhibit a dynamical tunneling between two UDOs' regular state.

[1] M. J. Davis and E. J. Heller, Quantum dynamical tunneling in bound states, J. Chem. Phys. **75**, 246 (1981).

[2] N. T. Maitra and E. J. Heller, Semiclassical perturbation approach to quantum reflection, Phys. Rev. A **54**, 4763 (1996).

[3] S. Keshavamurthy and P. Schlagheck, *Dynamical Tunneling: Theory and Experiment* (CRC Press, Boca Raton, FL, 2011).

[4] S. Tomsovic and D. Ullmo, Chaos-assisted tunneling, Phys. Rev. E **50**, 145 (1994).

[5] V. A. Podolskiy and E. E. Narimanov, Semiclassical description of chaos-assisted tunneling, Phys. Rev. Lett. **91**, 263601 (2003).

[6] A. Bäcker, R. Ketzmerick, S. Löck, and L. Schilling, Regular-to-chaotic tunneling rates using a fictitious integrable system, Phys. Rev. Lett. **100**, 104101 (2008).

[7] A. Bäcker, R. Ketzmerick, S. Löck, and N. Mertig, Fractional-power-law level statistics due to dynamical tunneling, Phys. Rev. Lett. **106**, 024101 (2011).

[8] A. Relaño, Chaos-assisted tunneling and $1/f^{\alpha}$ spectral fluctuations in the order-chaos transition, Phys. Rev. Lett. **100**, 224101 (2008).

[9] D. A. Steck, W. H. Oskay, and M. G. Raizen, Observation of chaos-assisted tunneling between islands of stability, Science **293**, 274 (2001).

[10] S. D. Frischat and E. Doron, Dynamical tunneling in mixed systems, Phys. Rev. E **57**, 1421 (1998).

[11] W. A. Lin and L. E. Ballentine, Quantum tunneling and chaos in a driven anharmonic oscillator, Phys. Rev. Lett. **65**, 2927 (1990).

[12] E. Doron and S. D. Frischat, Semiclassical description of tunneling in mixed systems: Case of the annular billiard, Phys. Rev. Lett. **75**, 3661 (1995).

[13] O. Brodier, P. Schlagheck, and D. Ullmo, Resonance-assisted tunneling in near-integrable systems, Phys. Rev. Lett. **87**, 064101 (2001).

[14] P. J. Richens and M. V. Berry, Pseudointegrable systems in classical and quantum mechanics, Physica D **2**, 495 (1981).

[15] E. Gutkin, Billiards in polygons, Physica D **19**, 311 (1986).

[16] T. Cheon and T. D. Cohen, Quantum level statistics of pseudointegrable billiards, Phys. Rev. Lett. **62**, 2769 (1989).

[17] A. Shudo, Y. Shimizu, P. Šeba, J. Stein, H.-J. Stöckmann, and K. Życzkowski, Statistical properties of spectra of pseudointegrable systems, Phys. Rev. E **49**, 3748 (1994).

[18] T. Shigehara, Conditions for the appearance of wave chaos in quantum singular systems with a pointlike scatterer, Phys. Rev. E **50**, 4357 (1994).

[19] J. Wiersig, Spectral properties of quantized barrier billiards, Phys. Rev. E **65**, 046217 (2002).

[20] E. B. Bogomolny, U. Gerland, and C. Schmit, Models of intermediate spectral statistics, Phys. Rev. E **59**, R1315 (1999).

[21] E. Bogomolny, O. Giraud, and C. Schmit, Periodic orbits contribution to the 2-point correlation form factor for pseudo-integrable systems, Commun. Math. Phys. **222**, 327 (2001).

[22] E. B. Bogomolny and C. Schmit, Structure of wave functions of pseudointegrable billiards, Phys. Rev. Lett. **92**, 244102 (2004).

[23] E. B. Bogomolny, Barrier billiard and random matrices, J. Phys. A **55**, 024001 (2022).

[24] E. B. Bogomolny and C. Schmit, Spectral statistics of a quantum interval-exchange map, Phys. Rev. Lett. **93**, 254102 (2004).

[25] E. B. Bogomolny, R. Dubertrand, and C. Schmit, Spectral statistics of a pseudo-integrable map: The general case, Nonlinearity **22**, 2101 (2009).

[26] B. I. Shklovskii, B. Shapiro, B. R. Sears, P. Lambrianides, and H. B. Shore, Statistics of spectra of disordered systems near the metal-insulator transition, Phys. Rev. B **47**, 11487 (1993).

[27] V. E. Kravtsov, I. V. Lerner, B. L. Altshuler, and A. G. Aronov, Universal spectral correlations at the mobility edge, Phys. Rev. Lett. **72**, 888 (1994).

[28] T. A. Brody, A statistical measure for the repulsion of energy levels, Lett. Nuovo Cimento **7**, 482 (1973).

[29] F. M. Izrailev, Simple models of quantum chaos: Spectrum and eigenfunctions, Phys. Rep. **196**, 299 (1990).

[30] E. Vergini and M. Saraceno, Calculation by scaling of highly excited states of billiards, Phys. Rev. E **52**, 2204 (1995).

[31] A. Barnett, Dissipation in deforming chaotic billiards, Ph.D. thesis, Harvard University, 2001.

[32] H. P. Baltes and E. R. Hilf, *Spectra of Finite Systems* (BIWissenschaftsverlag, Mannheim, 1976).

[33] K. Husimi, Some formal properties of the density matrix, Proc. Phys. Math. Soc. Jpn. **22**, 264 (1940).

[34] Z. Wang, J. Feng and B. Wu, Microscope for quantum dynamics with Planck cell resolution, Phys. Rev. Res. **3**, 033239 (2021).

[35] E. Wigner, On the quantum correction for thermodynamic equilibrium, Phys. Rev. **40**, 749 (1932).

[36] A. Bäcker, S. Fürstberger, and R. Schubert, Poincaré Husimi representation of eigenstates in quantum billiards, Phys. Rev. E **70**, 036204 (2004).

[37] W. A. Veech, Teichmüller curves in moduli space, Eisenstein series and an application to triangular billiards, Invent. Math. **97**, 553 (1989).

[38] E. B. Bogomolny, B. Dietz, T. Friedrich, M. Miski-Oglu, A. Richter, F. Schäfer, and C. Schmit, First experimental observation of superscars in a pseudointegrable barrier billiard, Phys. Rev. Lett. **97**, 254102 (2006).

[39] S. Åberg, T. Guhr, M. Miski-Oglu, and A. Richter, Superscars in billiards: A model for doorway states in quantum spectra, Phys. Rev. Lett. **100**, 204101 (2008).

[40] M. V. Berry and M. Robnik, Semiclassical level spacings when regular and chaotic orbits coexist, J. Phys. A **17**, 2413 (1984).

[41] M. Wilkinson, Tunnelling between tori in phase space, Physica D **21**, 341 (1986).

[42] J. Jahnel, When is the (co)sine of a rational angle equal to a rational number? arXiv:1006.2938 [math.HO].

[43] Č. Lozej, G. Casati, and T. Prosen, Quantum chaos in triangular billiards, Phys. Rev. Res. **4**, 013138 (2022).